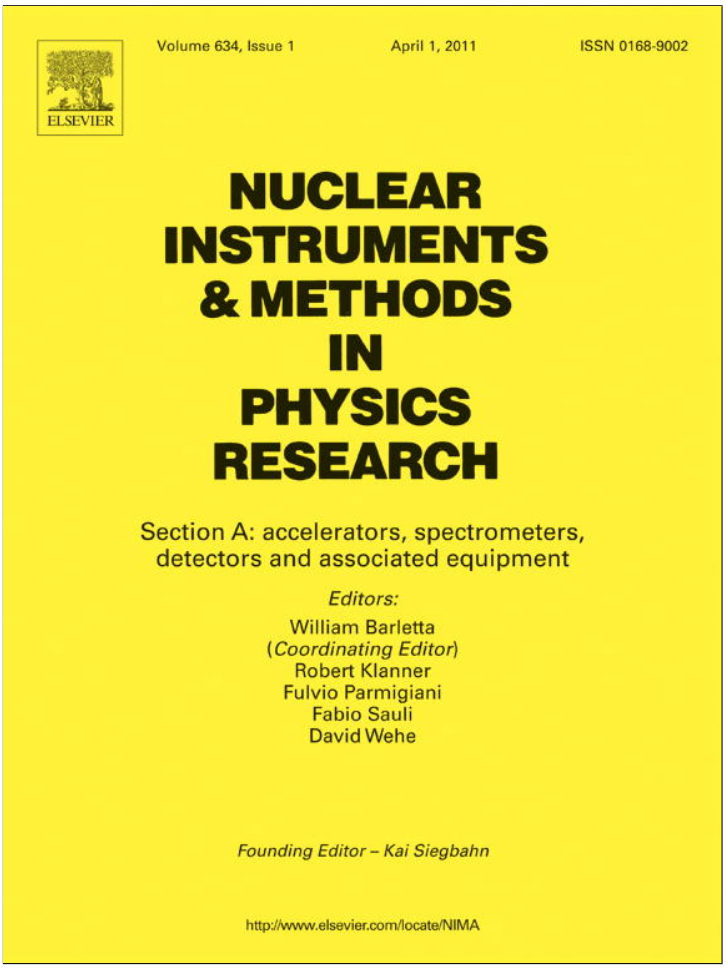

Nuclear Instruments and Methods in Physics Research A 634 (2011) 101–105

Contents lists available at ScienceDirect

Nuclear Instruments and Methods in Physics Research A

journal homepage: www.elsevier.com/locate/nima

Defective pixel map creation based on wavelet analysis in digital radiography detectors

Chun Joo Park [a], Hyoung Koo Lee [b], William Y. Song [a], Thorsten Graeve Achterkirchen [c], Ho Kyung Kim [d,*]

[a] Department of Radiation Oncology, University of California San Diego, 3855 Health Sciences Drive, La Jolla, CA 92093-0843, USA
[b] Department of Mining and Nuclear Engineering, Missouri University of Science and Technology, 210 Fulton Hall, 310 West 14th St., Rolla, MO 65409-0170, USA
[c] Rad-icon Imaging, DALSA Corporation, Sunnyvale, CA 94085, USA
[d] School of Mechanical Engineering, Pusan National University, Jangjeon-dong, Geumjeong-gu, Busan 609-735, Republic of Korea

ARTICLE INFO

Article history:
Received 9 April 2010
Received in revised form
8 January 2011
Accepted 10 January 2011
Available online 20 January 2011

Keywords:
CMOS
Defective pixel map
Digital radiography
Flat-panel detector
Wavelet transformation
X-ray

ABSTRACT

The application of digital radiography detectors has attracted increasing attention in both medicine and industry. Since the imaging detectors are fabricated by semiconductor manufacturing process over large areas, defective pixels in the detectors are unavoidable. Moreover, the radiation damage due to the routine use of the detectors progressively increases the density of defective pixels. In this study, we present a method of identifying defective pixels in digital radiography detectors based on wavelet analysis. Artifacts generated due to wavelet transformations have been prevented by an additional local threshold method. The proposed method was applied to a sample digital radiography and the result was promising. The proposed method uses a single pair of dark and white images and does not require them to be corrected in gain-and-offset properties. This method will be helpful for the reliable use of digital radiography detectors through the working lifetime.

1. Introduction and background

In recent years, mature electronics and manufacturing methods have led to many approaches for the design and construction of digital detectors for X-ray imaging [1]. Although various configurations of detectors are available, most detectors are mainly composed of two components: X-ray converters, such as scintillators (to provide "indirect" detection of X-rays by converting the detected X-ray energy into optical photons) or photoconductors (to provide "direct" detection of X-rays by converting the detected X-ray energy into electron–hole pairs), and readout pixel arrays [2,3]. As an optical-photon readout pixel array, charge-coupled devices (CCDs) have been used for a long time because of their high-quality, low-noise imaging performance [4]. Complementary metal-oxide–semiconductor (CMOS) technologies with their recent advances have become an alternative to CCDs, offering a great cost advantage and high physical performance [5]. Presently, flat-panel imagers based on arrays of hydrogenated amorphous silicon (*a*-Si:H) thin-film transistors in combination with either *a*-Si:H photodiodes (for indirect detection of X-rays) or storage capacitors (for direct detection of X-rays) are central for digital radiography, especially for large-area imaging applications [3,6]. All of these X-ray imaging detectors utilize pixel formats; hence they provide the intrinsic two-dimensional (2D) imaging capability.

These pixel array detectors are typically fabricated by the semiconductor manufacturing process. During fabrication, the non-uniform fabrication conditions over the areas of the pixel array, for example, the difference in doping concentrations in individual pixel elements, are unavoidable, and these conditions worsen as the detector size increases [7]. Unpredictable local defects can also occur in individual pixels or partial or complete lines [8]. These defective pixels defined as the pixels whose signal levels are abnormal from their neighbors, however, are normally accepted to a certain extent in commercial detectors. It is noted that local imperfections in the X-ray converters, such as scintillators and photoconductors, may also be observed as defective pixels in X-ray images.

Basically these defects are considered as fixed-pattern noise (FPN), which degrades the image quality. Image information is lost in radiography from individual pixels or from partial or complete lines [9], and severe streak and ring artifacts arise in computed tomography [10]. Therefore, clinical or industrial detectors have to recognize defective pixels (including line defects) and correct them to ensure optimal detector efficiency and image accuracy. Software processing is usually employed for correction. Above all, the exact and reliable identification of defective pixel locations is primary. However, the defective pixels in a detector may not be stationary in time and space [9]. Routine

* Corresponding author. Tel.: +82 51 510 3511; fax: +82 51 518 4613.
E-mail address: hokyung@pusan.ac.kr (H.K. Kim).

0168-9002/$ - see front matter © 2011 Elsevier B.V. All rights reserved.
doi:10.1016/j.nima.2011.01.037

use of detectors and thus the accumulated radiation damage progressively increase the density of defective pixels [9,11]. Therefore, the frequent evaluation of defective pixels is the only way to use a detector reliably [11].

In general, defective pixels are identified with dark (in the absence of X-rays) and white (under X-ray irradiation with no object) images. The dark and white images are also referred to as the offset and flat-field images, respectively. When there is no signal variation over large physical areas of a detector, the simple thresholding method with the global mean and standard deviation of the pixel values may be used to recognize defective pixels because defective pixels usually exhibit intensity values abnormally outside the mean value.

However, most detectors show unwanted, large-scale signal variations over areas, which worsen through the working lifetime of the detectors. Signal variation in the dark and white images is most likely caused by the readout amplifiers connected to the columns of the detector panel. Because the readout amplifiers are usually CMOS circuits, they probably exhibit small gain-and-offset variations, both column-to-column and across each amplifier chip. The exact nature of the non-uniformity depends on the particular device, but it is typically caused by parasitic capacitances and resistances that can vary as a function of how far a particular column is away from the power supply or the output amplifier. For example, if a column amplifier is connected to the output amplifier by a metal trace, the resistance of that trace will be proportional to its length. On a large device, this dependence can be significant and can affect the transfer gain for the signal coming from the column amplifier. Obviously, a column that is close to the output will have less parasitic resistance than one that is far away. It is noted that the variations in thickness of the X-ray converters can also give rise to variable intensity output in X-ray images.

X-ray equipment can also cause flaws and field variations, such as the heel effect, which is an intensity falloff on the anode side of the X-ray tube in the X-ray projection image, and which usually contributes as large-scale non-uniformities or low-spatial-frequency components in the Fourier domain of images.

These field variations can be dramatically improved by subtracting an offset (dark) image from the image to be corrected, and then dividing it pixel-to-pixel by an offset-corrected flat-field (white) image [12]. This gain-offset or flat-field calibration is a typical procedure in digital radiography. The flat-field calibration requires many dark and white images to reduce the statistical uncertainties in the pixel values during arithmetic operations. Considering the amount of potential drift of the detector response, the flat-field calibration should be frequently performed. It should be noted that only calibration with updated dark and white images can provide adequate images [11]. Moreover, the polyenergetic X-ray spectrum basically makes flat-field calibration incomplete because the pixel response is dependent on the energy and each pixel response in the image with an object is different with that in the offset-corrected flat-field image due to the beam-hardening effect [13].

In this study, a simple method of identifying defective pixels based on wavelet analysis is presented. The proposed method is motivated from the fact that the response of defective pixels is impulsive and the wavelet transform can decompose discontinuities and sharp spikes in functions. Therefore, the method is immuned to the influence of a global intensity variation; so it does not require flat-field-corrected images with many measurements, but may require a single pair of dark and white images.

2. Materials and methods

Defective pixels usually exhibit singular responses, unlike normal pixels in a detector. Therefore, sorting out these impulsive responses from global signal variations is the key in the identification of defective pixels. For this procedure, wavelet analysis is employed because the low-frequency components in an image can be easily identified and isolated by wavelet transformation. Conversely, wavelet transforms well represent the functions that have discontinuous and sharp peaks. Moreover, wavelet transforms can accurately deconstruct and reconstruct finite, non-periodic and/or non-stationary signals.

Wavelet transform is a linear combination of atomic decomposition, known as wavelets, especially for non-stationary functions [14]. Functions with discontinuities and functions with sharp spikes usually take much fewer wavelet basis functions than sine–cosine basis functions (e.g. Fourier transforms) to achieve a comparable approximation. Since first introduced in the early 1980s, the wavelet transform has become an important technique in signal or image processing, such as data compression, noise suppression, feature extraction, etc. [15].

2D image function $f(x, y)$ of $M \times N$ pixels in size can be expressed as [14]

$$f(x,y) = \frac{1}{\sqrt{MN}} \sum_m \sum_n W_\varphi(j_0,m,n)\varphi_{j_0,m,n}(x,y) + \frac{1}{\sqrt{MN}} \sum_{k=H,V,D} \sum_{j=j_0}^{\infty} \sum_m \sum_n W_\psi^k(j,m,n)\psi_{j,m,n}^k(x,y), \quad (1)$$

where j_0 is an arbitrary starting scale and the $W_\varphi(j_0,m,n)$ coefficients define an approximation of $f(x, y)$ at scale j_0. The $W_\psi^k(j,m,n)$ coefficients add horizontal, vertical, and diagonal details for scales $j \geq j_0$ and the superscript k denotes the direction; H, V, and D represent horizontal, vertical, and diagonal directions, respectively. m and n designate the sizes of the sub-images and depend on the applied scales. φ and ψ are basis functions, and they are

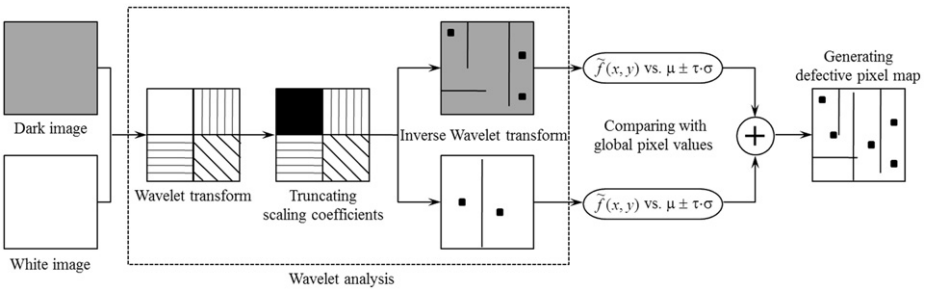

Fig. 1. A sketch illustrating the procedure for generating a defective pixel map based on wavelet analysis. Each of the dark and white images is changed into a multi-scale sub-image by wavelet transformations. Among four sub-images, the one describing scaling coefficients, which contains low-frequency band characteristics, is truncated and padded with zeros. The modified image is then turned back by inverse transformation, and it only contains sharp speckles. The abnormal singular signal distribution is checked by comparing it with the local pixel mean and its standard deviation, and finally identified as defective pixels.

called scaling and wavelet functions, respectively. If we can select the scaling coefficients of an image and modify them, i.e. replace them by zeros, we can obtain an image $\tilde{f}(x,y)$ without global signal variations.

The identification method of defective pixels including line defects is schematically illustrated in Fig. 1. The wavelet transform is applied to a dark image. The transformed image is then represented as four sub-images. In order to suppress or remove the large-scale signal variations, the sub-image represented by scaling coefficients is truncated. In other words, the pixel values consisting of the sub-image are replaced by zeros. And then, the inverse wavelet transform is applied. The reconstructed image is now a filtered image of low-spatial-frequency components and it clearly shows singularities, such as spikes and discontinuities in the pixel values. We used the Haar function as a wavelet [14]. For ensuring defective pixels, the surrounding pixel values were checked again with the local pixel mean μ, its standard deviation σ, and threshold level τ (viz. $\mu \pm \tau\sigma$). This thresholding procedure may suppress misleads of temporal random pixel responses. The pixel locations of the defective pixels detected are mapped to a template. The defective pixel map is completed after repeated procedures on a white image.

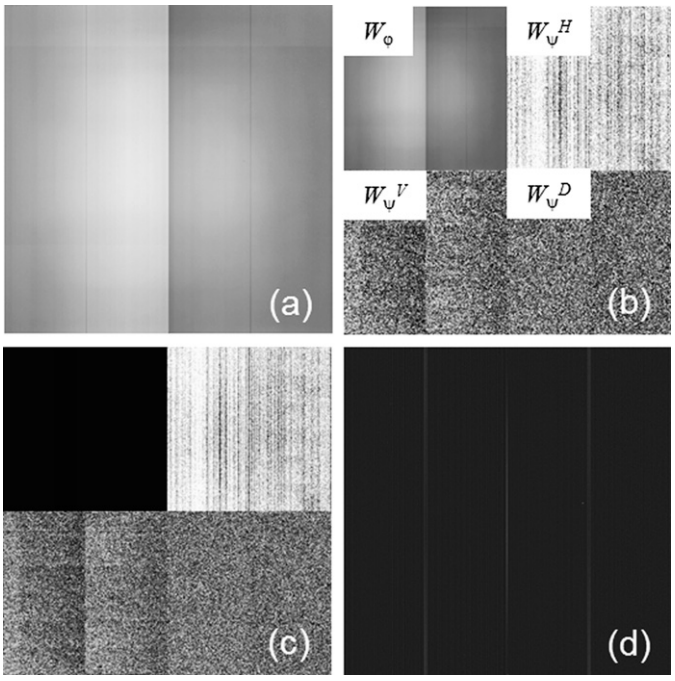

Fig. 2. Visual illustration of wavelet analysis to identify defective pixels. (a) A dark image obtained from the CMOS detector. (b) Representation of one-scale decomposition by wavelet transform. (c) One-scale decomposition with selected coefficients deleted. (d) Reconstructed image by inverse wavelet transform.

In this study, with the determined defective pixel map, digital radiography was corrected by simple adaptive median filtering. The mask size of the median filter was 5×5 pixels.

In order to demonstrate the proposed method to identify defective pixels in digital radiography, we implemented the method to an X-ray imaging detector. The detector was composed of photodiode arrays and overlying luminescent phosphor. The phosphor (Min-R^{TM}, Carestream Health, Inc., USA) is mainly made of a terbium-doped gadolinium oxysulfide (Gd_2O_2S:Tb) and it converts into optical photons, whose number is proportional to the absorbed energy of X-rays. The photodiode array made by CMOS process (RadEye^{TM}, Rad-icon Imaging Corp., USA) has a format of 512×1024 pixels with a pixel pitch of 48 μm [16]. Since only one narrow side of the CMOS photodiode array incorporates the readout electronics, two CMOS photodiode arrays were tiled side-by-side, and therefore, the actual format was 1024×1024 pixels and the field-of-view (FOV) was about $50 \times 50\ mm^2$. X-ray irradiation was performed with a small X-ray tube employing a tungsten target (Series 5000 Apogee, Oxford Instruments, USA). The operation conditions were a target voltage of 45 kV and cathode current of 1.0 mA. For sample images, humanoid hand phantom images were acquired. Due to the FOV of the detector, a part of phantom was imaged.

The detector has been used in our laboratory for a long time (more than three years). Since an FPN (including "ghosts" of high contrast objects) is linearly emphasized to the absorbed dose, the detector shows scabbed dark and white images. Therefore, finding defective pixels from the backgrounds was challenging.

3. Results

Wavelet analysis of a dark image obtained from the CMOS detector operated at an integration time of 550 ms is visually illustrated in Fig. 2. As shown in Fig. 2(a), the 2D display of the dark image shows non-uniform distribution of pixel dark currents and distinct, different responses of the two photodiode arrays. Fig. 2(b) represents the decomposed sub-images by one-scale wavelet transform. Fig. 2(d) shows the reconstructed image by the inverse wavelet transform after truncation of the scaling coefficients, as shown in the second quadrant of Fig. 2(c). In this image, the global signal variations are removed and only singularities are shown. The dark images before and after wavelet analysis can be more apparently demonstrated by a three-dimensional (3D) display, as shown in Fig. 3(a) and (c), respectively. Fig. 3(b) is a 3D plot of the white image. The large pits of the central region in the dark and white images are the ghosting resulting from the persistent local irradiation of X-rays during the usage of the detector.

One-dimensional profiles extracted from 2D images in the row (or address) direction before and after wavelet analysis are compared in Fig. 4. Truncation of the scaling coefficients in wavelet domain effectively removes the low-spatial-frequency components in an image; hence, singularities are easily identified.

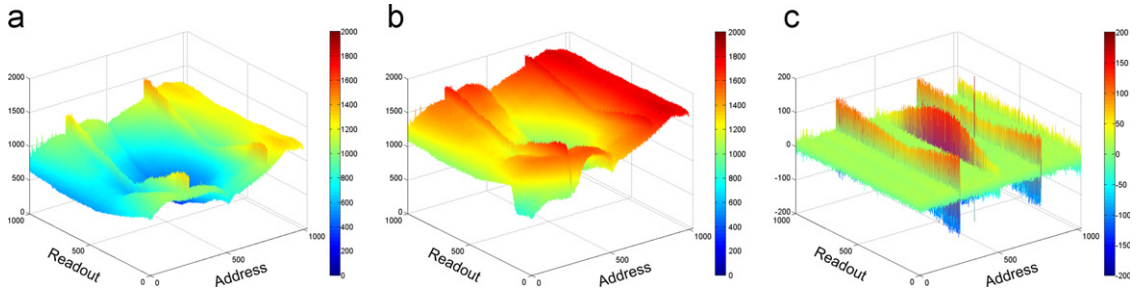

Fig. 3. 3D displays of detector signals before and after wavelet transformation. (a) and (b) Signal distributions of the dark and white images, respectively. (c) Dark image after wavelet analysis.

Fig. 5 shows defective pixel maps generated by wavelet analysis. Fig. 5(a) and (b) shows the maps for the dark and white images, respectively. The map from the dark image has three defective lines while that from the white image has one defective line. Some of defective lines are composed of more than a single line. The total defective pixel map considering both the dark and white images are shown in Fig. 5(c). In order to observe the behavior of pixel defects, arbitrarily selected regions were investigated. For easier visualization, the regions are displayed by negative transformation and the display is enlarged by a factor 2. Regions *D*1 and *W*1 are the same regions of the maps of the dark and white images, respectively. Regions *D*2 and *W*2 also reflect the same regions in the maps of the dark and white images. Comparing *D*1 and *W*1, some of defective pixels share the same position both in the dark or white maps, but some do not because of the small abnormality in the signal intensity in the white image compared with the global mean pixel value. As shown in the selected regions of *D*2 and *W*2, some defective pixels are very sensitive to X-ray exposure. It should be noted that the defective pixels are clustered in the map obtained from the white image, probably due to the signal leakage of the defective pixel into its neighborhood.

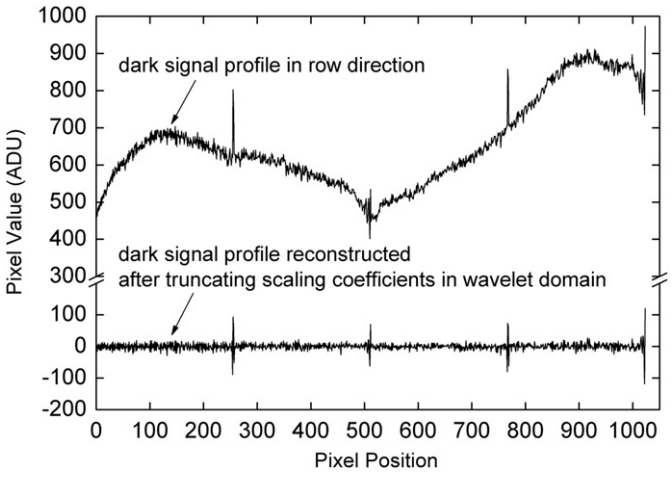

Fig. 4. Comparative signal profiles before and after wavelet analysis.

The defective pixel map that was obtained was used to correct defective pixels on a hand phantom image, as shown in Fig. 6. Simple adaptive filtering worked well, as shown in Fig. 6(b). The line defects indicated as arrows in Fig. 6(a) are not shown in Fig. 6(b). The region indicated as a dotted box in Fig. 6(a) has been investigated in detail, as shown in Fig. 7. The arrows in Fig. 7(a) indicate two pixel defects and one line defect. As shown in Fig. 7(b), two pixel defects are clearly corrected but a faint line seam is still shown. Fig. 7(c) is a difference image between Fig. 7(a) and (b).

4. Discussion and conclusion

In the wavelet transforms, we used the Haar function as a wavelet. The Haar function provides an operation similar to the derivative when finding directional wavelet coefficients. Therefore, there might

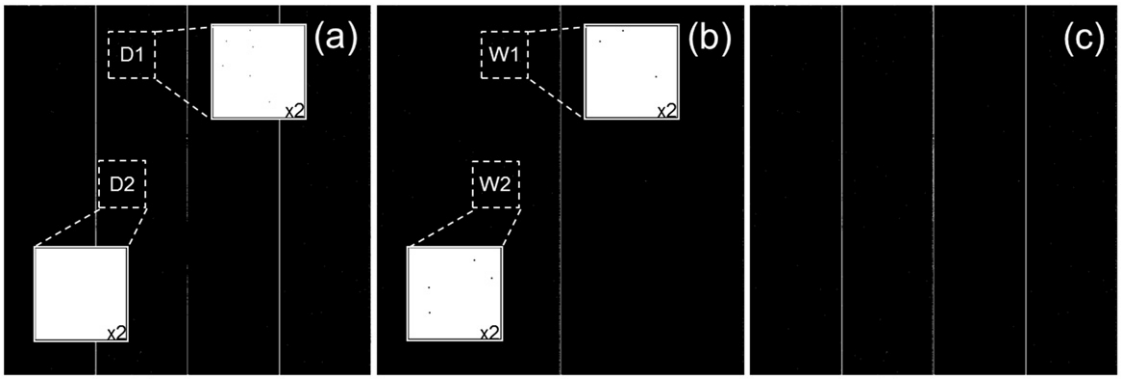

Fig. 5. Templates mapping defective-pixel locations. (a) and (b) are the defective pixel maps obtained from the dark and white images, respectively. (c) is the complete defective pixel map by combining (a) and (b). Insets are the enlarged images, displayed in negative, for the regions indicated by the dotted boxes.

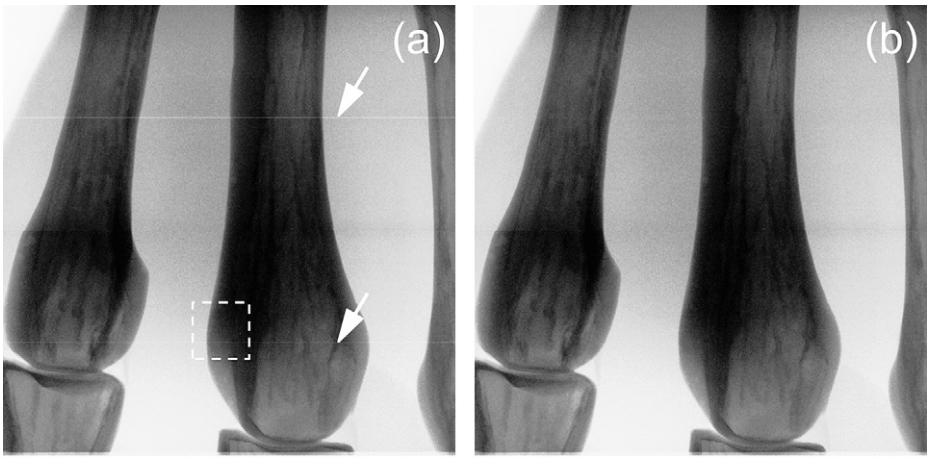

Fig. 6. Example of defective-pixel correction in digital radiography with the defective pixel map. (a) An image of hand phantom obtained from the CMOS detector. (b) Defect-corrected image by adaptive median filtering operation based on the defective pixel map.

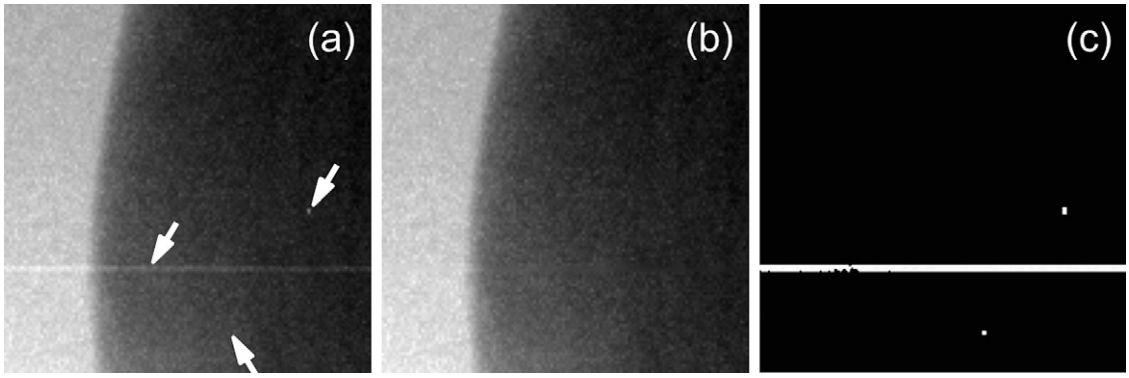

Fig. 7. Enlarged images indicated by the dotted box in Fig. 6(a). (a) and (b) Images before and after the defective-pixel correction, respectively. (c) Difference between (a) and (b).

be artifacts around the reconstructed singularities. As shown in Fig. 4, the profile after wavelet transformations shows sharp spikes adjacent to the original singular responses in negative values. Threshold checking with the local mean value and standard deviation for the neighboring pixel values would prevent the negative spikes from defective pixels as performed in this study. Other filter functions, which would not cause this kind artifact, as a wavelet are alternatives. Although we partly employed the threshold method, the computational cost is chief because thresholding is applied to limited regions around singularities identified by wavelet analysis.

There are several techniques for defective pixel correction with various tradeoffs between the effectiveness and complexity of computations. The simplest method is to apply a median filter as demonstrated in this study. A similar method is mean filtering. While median filtering replaces the defective pixel with the median around pixel values, mean filtering uses the average value of the surrounding pixel values. Although mean filtering is more time-consuming than median filtering, the image quality is better because it uses information from more than just one of the neighboring pixels. In mean filtering, however, the neighboring pixels need to be good pixels.

Unlike isolated defective pixels in space, clustered pixel defects are serious because of the lack of information for correction. Aach and Metzler [17] introduced an iterative deconvolution method in the frequency domain. They modeled a distorted radiography due to defective pixels by a multiplication of the undistorted radiography by the defective pixel map. Then, defect interpolation would correspond to the deconvolution of the corresponding spectra. Although this method has high computational complexity, it is particularly suited to large defective areas. With respect to line defect interpolation, various interpolation techniques are available [18].

Defective pixels are an inevitable result of the manufacturing process for large-area semiconductor digital detectors. For the reliable use of detectors over their working lifetimes, a complete list of the locations of all the defective pixels (or a defective pixel map) should be prepared, and the defective pixel map needs to be updated by frequent monitoring. In this study, we introduced the generation of a defective pixel map based on wavelet analysis and applied the map to the digital radiography. The method does not require gain-and-offset-corrected images. Therefore, it is appropriate to periodic monitoring of digital radiography detectors.

Acknowledgment

This work was supported by a Grant-in-Aid for Strategy Technology Development Program (no. 10032060) funded by Ministry of Knowledge Economy (MKE, Korea).

References

[1] M.J. Yaffe, J.A. Rowlands, Phys. Med. Biol. 42 (1997) 1.
[2] J. Yorkston, Nucl. Instr. and Meth. A 580 (2007) 974.
[3] H.K. Kim, I.A. Cunningham, Z. Yin, G. Cho, Int. J. Precis. Eng. Manuf. 9 (2008) 86.
[4] S.M. Gruner, M.W. Tate, E.F. Eikenberry, Rev. Sci. Instr. 73 (2002) 2815.
[5] M. Bigas, E. Cabruja, J. Forest, J. Salvi, Microelectron. J. 37 (2006) 433.
[6] H.G. Chotas, J.T. Dobbins III, C.E. Ravin, Radiology 210 (1999) 595.
[7] P. Munro, D.C. Bouius, Med. Phys. 25 (1998) 689.
[8] M. Farrier, T. Graeve Achterkirchen, G.P. Weckler, A. Mrozack, IEEE Trans. Electron Dev. ED-56 (2009) 2623.
[9] R. Padgett, C.J. Kotre, Phys. Med. Biol. 49 (2004) 977.
[10] H.K. Kim, S.C. Lee, M.H. Cho, S.Y. Lee, G. Cho, IEEE Trans. Nucl. Sci. NS-52 (2005) 193.
[11] H.K. Kim, M.K. Cho, T. Achterkirchen, W. Lee, IEEE Trans. Nucl. Sci. NS-56 (2007) 1179.
[12] A.L.C. Kwan, A. Seibert, J.M. Boone, Med. Phys. 33 (2006) 391.
[13] D.W. Davidson, C. Fröjdh, V. O'Shea, H.-E. Nilsson, M. Rahman, Nucl. Instr. and Meth. A 509 (2003) 146.
[14] R.C. Gonzalez, R.E. Woods, Digital Image Processing, Prentice-Hall, Inc., Upper Saddle River, NJ, 2002.
[15] M.D. Harpen, Med. Phys. 25 (1998) 1985.
[16] T. Graeve, G.P. Weckler, Proc. SPIE 4320 (2001) 68.
[17] T. Aach, V. Metzler, Proc. SPIE 4322 (2001) 824.
[18] F. Xu, H. Liu, G. Wang, B.A. Alford, J. Electron. Imag. 9 (2000) 22.